Pipe Viscometer for Continuous Viscosity and Density Measurement of Oil Well Barrier Materials

V. N. Lima[1,2], E. Randeberg[1]*, A. Taheri[1], and H. J. Skadsem[1,3]

[1]NORCE Norwegian Research Centre AS
[2]Pontificia Universidade Catolica do Rio de Janeiro (PUC-Rio)
[3]University of Stavanger

Summary

The barrier material is a crucial component for wells, as it provides mechanical support to the casing and prevents the uncontrolled flow of formation fluids, ensuring zonal isolation. One of the essential prerequisites for the success of cementing an oil and gas well is the efficient removal of in-situ fluids and their adequate replacement by the barrier material. The quality of the mud displacement is affected by both the density and the viscosity hierarchy among subsequent fluids. Consequently, accurate and reliable measurement of fluid properties can help ensure consistent large-scale mixing of cementing fluids and verification that the properties of the mixed fluid are according to plan. In this paper, we investigate the implementation of a pipe viscometer for future automated measurements of density and viscosity of materials for zonal isolation and perform a sequential validation of the viscometer that starts with small-scale batch mixing and characterization of particle-free calibration liquids, followed by conventional Class G cement and selected new barrier materials. Finally, a larger-scale validation of the pipe viscometer was performed by integrating it into a yard-scale batch mixer for in-line characterization of expanding Class G oilwell cement mixing. In all cases, flow curves derived from pipe viscosity measurements were compared with offline measurements using a rheometer and a conventional oilfield viscometer. After a series of measurements and comparisons, the investigated in-line measurement system proved adequate for viscosity estimation. The flow curve of the barrier materials showed results similar to measurements using a conventional viscometer, validating the proposed test configuration to continuously measure the rheological behavior of the barrier material. The pipe viscometer flow curves are generally found to be in good quantitative agreement with independent viscometer characterization of the fluids, although some of the pipe viscometer measurements likely exhibited entrance length effects. Future improvements to the pipe viscometer design involve the assessment of even longer pipe sections to allow full flow development at the highest shear rate range and possibly different pipe diameters to improve the measurement resolution of low-shear rate viscosity.

Introduction

The oil well cementing process involves placing cement slurries in the annular space between the casing and the rock formation. After placement, the cement hardens to form a hydraulic seal in the wellbore, preventing the migration of formation fluids into the annulus. In the placement process, the cement paste flows through the interior of the casing into the annular space that is to be cemented, displacing in-situ fluids as it is pumped toward the surface. Because the drilling mud or the existing fluids can affect zonal isolation and the bonding of the cement to the casing or rock formation walls, one of the essential prerequisites for the success of cementing an oil and gas well is the efficient removal of these fluids and their adequate replacement by the barrier material.

The placement of well barrier materials for zonal isolation behind casings (primary cementing) or for plug cementing is affected by geometrical parameters (inclination, casing eccentricity, and diameter ratio) and by several competing forces, including inertia, viscous stresses, buoyancy, and also interfacial tension in the case of immiscible fluid pars. The relative magnitude of several of these forces is directly affected by the viscosity and density of the cementing fluids and the fluid to be displaced. Based on the insights of early experimental investigations of annular fluid displacements, Couturier et al. (1990) suggested a set of compact design rules for effective laminar flow displacements in vertical and inclined annuli. These design rules promote a density and a viscosity hierarchy among the fluids, (i.e., favoring a stable fluid configuration where the denser and more viscous fluid displaces a lighter and lower viscosity fluid). The design rules also reflect casing eccentricity (favoring centralized casing) and a requirement for fluid flow along the narrow side of the annulus, which is linked to the yield stress property of viscoplastic fluids (Couturier et al. 1990; Théron et al. 2002; Pelipenko and Frigaard 2004). The impact of fluid viscosity on annular displacements is also key in the cementing of horizontal sections, where the existence of steady laminar displacements is primarily determined by the rheological hierarchy and casing eccentricity (Carrasco-Teja et al. 2008). The density and rheology of the cementing fluids are also affecting the local flow regime (i.e.. whether the fluids are flowing mainly in a laminar, transitional, or turbulent regime). As both the flow regime and the relative magnitude of the forces that affect the displacement quality are linked to fluid density and viscosity, accurate fluid characterization at the rigsite is important.

Modern cementing units are equipped with monitoring devices for continuous measurement of volumetric flow, density, and pump pressure. The viscosity of the mixed fluid is normally measured by manual fluid sampling and using an oilfield Couette viscometer to obtain the viscosity at fixed wall shear rates, following practices recommended by the American Petroleum Institute (API). Conventional oilfield viscometers provide shear rate conditions that span at least two orders of magnitude and cover shearing conditions that are relevant for downhole placement of cement. Further, since the measurement protocol specified by API includes upward and downward shear rate ramp with a specified time interval for measurement at each shear rate, qualitative information about thixotropic behavior can also be obtained.

*Corresponding author; email: erra@norceresearch.no

Original SPE manuscript received for review 22 March 2023. Revised manuscript received for review 24 May 2023. Paper (SPE 215833) peer approved 1 June 2023.

Several studies in the literature have explored in-line measurements using pipe viscometers for automated fluid characterization. Focusing on several Class H oilwell cement pastes, Bannister (1980a) compared flow curves measured with a 12-speed Fann 35 Couette viscometer to corresponding flow curves derived from a pipe viscometer consisting of interchangeable pipes with diameters ranging from 2.1 mm to 7.7 mm (0.083 in. to 0.305 in.) and lengths ranging from 152 mm to 1219 mm (6 in. to 48 in.). While the flow curves obtained for a simple fluid (constant viscosity oil) showed excellent agreement between the two viscometers, the difference was found to be more significant for oilwell cements. In addition, Bannister (1980b) reported that flow curves obtained with the pipe viscometer displayed a dependency on the inner piper diameter, which suggests that particle migration and wall slip affected the friction pressure measurements in the relatively small-diameter pipes used (Bannister 1980a; Bannister and Benge 1981). A comparison between Couette and pipe viscometer flow curves for a model cement paste was reported by Clark and Shaughnessy (1990), who used a model particle suspension instead of a hardening cement paste in their experiments. Flow curves derived from different diameter pipes [ranging from 7.7 mm (0.303 in.) to 10.74 mm (0.423 in.)] suggested an impact of wall slip and particle migration. While the mechanisms governing apparent wall slip remain to be fully understood, it is known that both steric depletion and particle migration will affect the local particle concentration adjacent to the walls (Wilms et al. 2022) and that the importance of slip decreases as the pipe diameter increases (Mannheimer 1991).

More recently, pipe viscometers have been developed and tested with the primary focus of continuously monitoring the density and viscosity of drilling fluids, either on a laboratory scale (Sui and Vidaur 2020) or by full-scale tests (Carlsen et al. 2013). Magnon and Cayeux (2021) studied pipe viscometer measurements of an aqueous polymeric solution and derived analytical results that correlate the wall shear rate to measurement of imposed flow rate, differential pressure, and Herschel-Bulkley fluid model parameters. Their work demonstrated how the viscosity function of the test fluid can be determined simultaneously with the wall shear rate and that the physics-based analytical solution can result in improved reliability, particularly for yield stress fluids (Magnon and Cayeux 2021). An investigation of the pipe viscometer accuracy was addressed by Liu et al. (2022), who proposed a setup with a pulsation damper and backpressure valve to stabilize flow rate and pressure. Moreover, they evaluated the size of pressure sensor ports and found that the optimal hole size should be close to 5 mm (0.197 in.) in diameter. This test configuration has been shown to be efficient even using acoustic measurements (Ofoche and Noynaert 2020); however, problems related to the intrinsic properties of fluids, such as thixotropy, may occur and impact the results. Because of this, more recent studies have evaluated the effects of thixotropy, pressure, and temperature on drilling fluids and their impact on tests using pipe rheometers (Cayeux and Leulseged 2020; Cayeux 2020). Cayeux and Leulseged (2020) observed that for thixotropic fluids, passing through a change in diameter can influence pressure gradients over substantial distances, and, therefore, the point where the pressure sensors are placed can significantly influence the quality of measurements. To reduce the influence of shear history, Gul et al. (2020a, 2020b) introduced a helical pipe viscometer system for automated mud measurements. In addition to reducing the footprint, this helical setup allowed the collection of more data in the laminar flow because of high frictional pressure losses and delayed transitions in the flow regime, which increases the accuracy of low-shear rheological parameter estimates.

Field cases were also explored in the literature. Gul et al. (2020c) showed that the characterization of the essential physical and chemical properties of drilling fluids (plastic viscosity, yield point, pressurized density, and oil/water ratio) could be performed at high frequency, considering the help of process automation using a tube viscometer. They emphasized that compared to conventional Couette-type viscometers, the tube viscometer is much less prone to clogging by solids in the fluid, and allows for the characterization of additional rheological parameters, such as the critical Reynolds number, which characterizes the transition of laminar to turbulent flow, and the friction factor in the turbulent flow regime. In addition to the points addressed by Gul et al. (2020c), Taugbøl et al. (2021) highlight the importance of automated measurements, including for offshore drilling rigs, giving high-quality real-time data of fluid density, and rheology that can be easily transferred to onshore operation centers for continuous surveillance of fluid properties. All of the work mentioned so far shows that fully automated fluid measurement is rapidly becoming a reality, considering drilling fluids. Its potential benefits to well construction operations include better hydraulic management, which is vital to optimizing drilling performance and optimizing fluid treatment and maintenance.

This paper describes the implementation of a pipe viscometer for automated measurements of well barrier materials, such as cement slurries and new alternative barrier materials. The pipe viscometer is designed to allow retrofitting it to the existing field-scale cement mixing units [i.e., batch mixers or mixing units for continuous ("on-the-fly") mixing of large cement paste volumes]. The pipe viscometer can therefore enable continuous measurement of cement paste density and viscosity as the paste is being mixed in batch mixers or as the paste is being pumped downhole in the case of continuous mixing operations. Once installed, the pipe viscometer can therefore facilitate documentation and quality assurance of these properties as the paste is placed in the well, and enable adjustments of paste composition and properties in the case of batch mixing operations. To facilitate such future field implementation, the physical footprint and simplicity of operation of the viscometer are emphasized.

The structure of this paper is as follows. We first detail the design and instrumentation of the pipe viscometer and discuss the conversion of flow rate and friction pressure measurements to a corresponding flow curve with no a priori assumptions pertaining to the fluid viscosity. We next perform a sequential validation of the proposed pipe viscometer, starting with small-scale batch mixing and characterization of particle-free calibration fluids, small-scale mixing of Class G oilwell cement paste and three alternative materials for zonal isolation, and finally integrating the pipe viscometer into a yard-scale batch mixer. The final test involves the mixing and in-line characterization of an expanding Class G oilwell cement paste. At all stages, the flow curves derived from the pipe viscometer are compared to equivalent flow curves obtained using a scientific rheometer or the industry-standard Fann 35 Couette viscometer.

Pipe Viscometer Design. Initially, in-line measurements were aimed at characterizing both viscosity and density using horizontal and vertical pipe sections in which pressure losses were recorded through two sets of pressure sensors **(Fig. 1).** This configuration consisted of a fluid mixing tank with an agitator, a progressive cavity pump (screw pump), and two pipe measuring sections, each 3 m (9 ft) long and with internal diameter $D = 0.0212$ m (0.835 in.). The inner pipe diameter is designed to be significantly larger than that used in the previous work on pipe viscometry of cementitious fluids in an effort to mitigate potential wall slip effects reported in those studies (Bannister 1980b; Bannister and Benge 1981; Clark and Shaughnessy 1990). The current pipe viscometer was instrumented with differential pressure sensors placed along the pipe sections, allowing continuous measurement of pressure loss due to friction in the horizontal section and a combination of pressure loss due to friction and hydrostatic pressure gradient in the vertical section. Thus, by subtracting the frictional pressure component, measured in the horizontal section, from the vertical pressure difference, which included the frictional and hydrostatic pressure components, it was possible to obtain a continuous measurement of both viscosity and density. It should also be noted that the differential pressure sensors used have a measurement range of up to 1300 millibars (18.85 psi) and are spaced 150 cm (4.92 ft) apart. The progressive cavity pump can operate up to pressures of 10 bar (145 psi) and at 175 rev/min without measurable pulsation effects. In addition, a temperature sensor to record temperature variations during measurements was placed in the mixing tank. Finally, a Coriolis flowmeter for density and flow measurement was placed between the mixing tank and the pump.

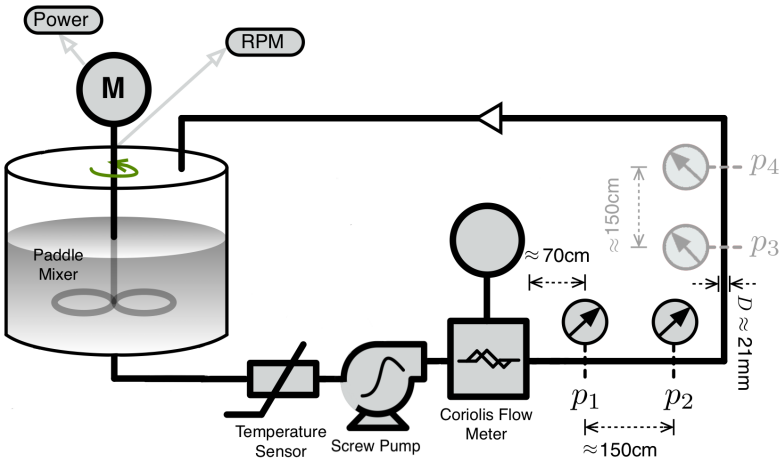

Fig. 1—Schematic drawing of the pipe viscometer test setup.

The pipe viscometer configuration shown in **Fig. 1** is considered representative of in-line density and viscosity measurements on the fluid recirculation line in a batch mixer. Finally, and as pointed out above, the main purpose of the second pair of differential pressure sensors (p_3 and p_4) is to enable measurement of the paste density. If the pipe viscometer is installed with a Coriolis flowmeter, as in **Fig. 1**, the pressure-based density measurement provided by the vertical part of the pipe is no longer required, and p_3 and p_4 may be omitted from the design. For completeness, we provide a comparison of density measurements from the Coriolis flowmeter and the vertical part of the recirculation line.

A laminar, fully developed flow is desired along the measurement sections of the pipe. Correlations that relate the pipe entrance length to the pipe diameter have been developed for different fluid viscosity models, including Newtonian (White 1991), power law (Poole and Ridley 2007), and Bingham fluids (Poole and Chhabra 2010). These correlations are often developed based on a generalized Reynolds number, Re_g, that ensures a Darcy-Weisbach friction factor $f = 64/\mathrm{Re}_g$ for fully developed laminar pipe flow. With this definition of Re_g, the ratio of development length to pipe diameter, X_D/D, is typically found to scale as $X_D/D \sim 0.0567\mathrm{Re}_g$ for high, laminar Reynolds numbers (White 1991; Poole and Ridley 2007; Poole and Chhabra 2010). In the limit of creeping flows, that is, $\mathrm{Re}_g \to 0$, a certain, nonzero entrance length is normally suggested, and this may be linked to, for example, the power law flow index, n (Poole and Ridley 2007), or the ratio of fluid yield stress to a characteristic shear stress scale (Poole and Chhabra 2010). In the current pipe viscometer design, the pipe measurement section starts 70 cm (2.3 ft) downstream of the Coriolis flowmeter, as shown in **Fig. 1**, corresponding to $X_D/D \approx 33$. This suggests that pipe flows with $\mathrm{Re}_g < 580$ can be considered fully developed at the start of the measurement section (White 1991).

When testing low-viscosity fluids, this criterion may be violated at higher imposed flow rates. To ascertain the flow development and eliminate measurements at conditions where the flow is likely not fully developed, we infer the generalized Reynolds number from measurements of the friction pressure gradient and the imposed flow rate through the Darcy-Weisbach friction factor. That is, since $f = 64/\mathrm{Re}_g$ by definition, we have $\mathrm{Re}_g = 8\rho\bar{u}^2/\tau_w$, where the bulk velocity $\bar{u} = Q/A$ is the imposed volumetric flow rate, Q, averaged over the pipe cross-sectional area, A, and τ_w is the pipe wall shear stress. In laminar conditions, this is linked to the measured (assumed fully developed) pressure gradient as follows: $\tau_w = (D/4)\Delta p/\Delta L$. In what follows, the fluid characterization is based on only those measurements that correspond to a "measured" generalized Reynolds number of $\mathrm{Re}_g < 580$.

To enable the characterization of fluid flow curves using established viscosity models, we convert simultaneous measurements of imposed flow rate and friction pressure gradient to the corresponding wall shear rate and wall shear stress. As discussed above, the wall shear stress is obtained from the differential pressure measurement. The corresponding wall shear rate is obtained using the Mooney-Rabinowitsch relation (Rabinowitsch 1929; Bird et al. 1987)

$$\dot{\gamma}_w = \frac{1}{\tau_w^2}\frac{\mathrm{d}}{\mathrm{d}\tau_w}\left(\tau_w^3\frac{Q}{\pi R^3}\right) = \frac{\dot{\gamma}_a}{4}\left(3 + \frac{\mathrm{d}\ln\dot{\gamma}_a}{\mathrm{d}\ln\tau_w}\right), \quad (1)$$

with R being the inner radius of the pipe and $\dot{\gamma}_a = 8\bar{u}/D$ being the Newtonian, or apparent, wall shear rate.

We evaluate the wall shear rate, $\dot{\gamma}_w$, by approximating $\mathrm{d}\ln\dot{\gamma}_a/\mathrm{d}\ln\tau_w$ to a polynomial, as illustrated in **Fig. 2.** Measurements of differential pressure and flow rate for an expanding cement paste are in this figure converted to corresponding wall shear stress and apparent wall shear rates and fitted using a second-order polynomial. For the fluids tested in this study, we find that (nonphysical) polynomial functions provide very good quantitative approximations to the physical measurements. The resulting polynomial approximations enable analytical expressions for the true wall shear rate, $\dot{\gamma}_w$, through Eq. 1 and result in a simple, iterative procedure for determining constitutive fluid model parameters using the resulting parameter-free flow curve. Based on the qualitative trend in the measurements of wall shear stress and the estimated wall shear rate, we model the test fluids as either Newtonian, power law, Bingham plastic, or Herschel-Bulkley fluids and determine the model parameters using simple least squares or, in the case of Herschel-Bulkley fluids, the Levenberg-Marquardt method (Press et al. 2001). As pointed out by Magnon and Cayeux (2021), however, extra care is required when fitting simple (nonphysical) polynomial functions to measurements acquired using fluids with significant yield stress. As most cementing fluids and alternative well barrier fluids exhibit yield stress behavior, an alternative approach to establish the flow curve from pipe viscometer data would be to make an a priori assumption concerning fluid model and determine wall shear rate and model parameters simultaneously, as per Magnon and Cayeux (2021).

Test Program. A staged approach to testing the designed pipe viscometer was undertaken, where initial tests were performed using small batches [50 L (13.2 gal)] of solids-free and nonhardening calibration fluids. For this purpose, a 90% weight concentration (W/W)

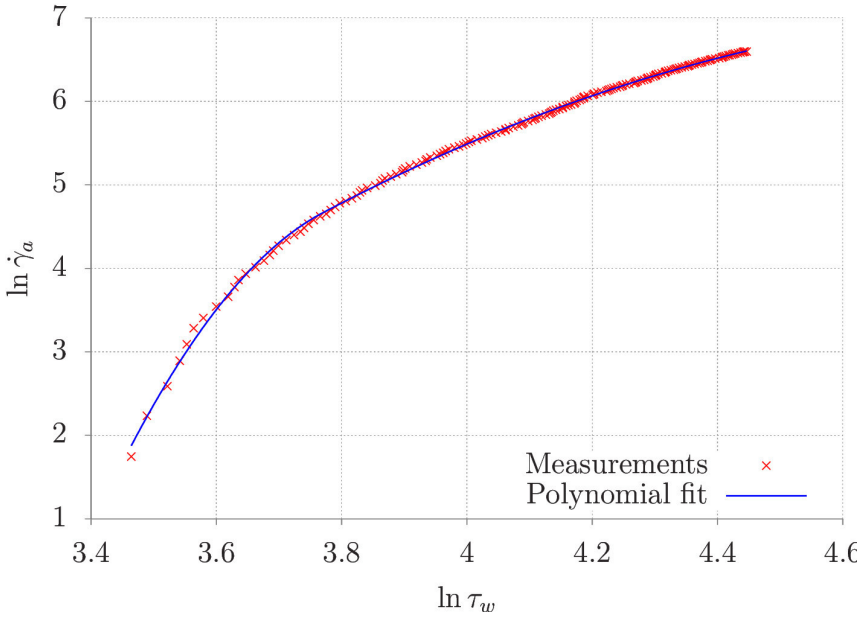

Fig. 2—Approximating the friction pressure gradient (wall shear stress) as a function of imposed flow rate by a smooth fourth-order polynomial facilitates the calculation of wall shear rates using Eq. 1.

glycerol-water solution was prepared as a Newtonian test fluid. A 3% weight concentration (W/W) liquid xanthan gum fluid was prepared as a highly shear-thinning non-Newtonian test fluid. The pipe viscometer rheograms, or flow curves, for these calibration fluids were compared to flow curves acquired using a scientific rheometer [Anton Paar MCR301; cone and plate measurement geometry (CP75)]. Further, the accuracy of the fluid density measurement acquired by combining the pressure measurements in the horizontal and vertical pipe segments was compared to continuous density measurements from a Coriolis flowmeter.

The next stage of testing was also performed using small fluid batches [50 L (13.2 gal)] and realistic well barrier fluids. For this purpose, conventional Class G oilwell cement and three alternative barrier materials were mixed and tested in the pipe viscometer. In this study, a self-healing cement, a corrosion-resistant cement, and a rock-based geopolymer were considered as alternative barrier materials. Mixing of the fluids was performed in the pipe viscometer arrangement shown in **Fig. 1** and was achieved by a submerged paddle in the mixing tank and, probably more importantly, by continuous recirculation provided by the positive displacement pump. The pump was operated at a speed corresponding to a flow rate of approximately 40 L/min (10.6 gal/min) during the mixing of the test fluid. For the fluids prepared this way, independent flow curve measurements were acquired using the oilfield standard Fann 35 Couette viscometer fitted with the R1-B1 concentric cylinder measurement geometry.

The third and final stage of testing involved fitting the pipe viscometer to a medium-scale batch mixer that has a design similar to full-scale cement batch mixers but with reduced volumetric capacity for the purpose of large-scale research and testing activities. A schematic of the medium-scale batch mixer and a discussion of the interfacing of the pipe viscometer to this mixer are provided in the medium-scale mixing test section. The pipe viscometer was operated during the mixing of 550 L (145.2 gal) of expanding Class G oilwell cement for the main purpose of cementing casing test sections in a separate project activity. The expanding cement paste was tested repeatedly during the conditioning stage of the batch mixing, and the pipe viscometer flow curves were compared to Couette viscometer measurements. An overview of the test fluids, and some of their key properties, is provided in **Table 1.** Recipes for the Class G and the expanding Class G cement pastes are provided in **Table 2.**

Test Phase	Fluids	Density	Free Fluid Test	Thickening Time (100 Bc)
Calibration (50 L batch volume)	Glycerol	1.25 s.g.	–	–
	Xanthan gum solution	0.98 s.g.	–	–
Small scale (50 L batch volume)	Class G cement paste	1.92 s.g.	0% (40ºC, angle 45º)	09:47 (40°C, 99 bar)
	Self-healing cement paste	1.95 s.g.	0% (21ºC, angle 90º)	04:36 (19°C, 60 bar)
	Corrosion-resistant cement paste	1.80 s.g.	0% (20ºC, angle 90º)	08:04 (65°C, 0 bar)
	Geopolymer paste	1.89 s.g.	0% (25ºC, angle 90º)	05:06 (30°C, 35 bar)
Medium scale (550 L batch volume)	Expanding Class G cement paste	1.92 s.g.	0% (40ºC, angle 45º)	07:20 (40°C, 99 bar)

Bc, Bearden consistency unit.

Table 1—Overview of fluids and their properties as used in the different phases of testing the pipe viscometer. Test conditions for the free fluid test (temperature and deviation angle) and thickening time measurement (temperature and pressure) are indicated in parentheses for the hardening fluids.

Ingredient	Class G Cement Paste	Expanding Class G Cement Paste
Class G cement	100% BWOC	100% BWOC
Fresh water	52.55 L/100 kg	54.05 L/100 kg
Defoamer	0.1 L/100 kg	0.1 L/100
Retarder	0.7 L/100 kg	0.7 L/100 kg
Suspension agent	0.02% BWOC	0.02% BWOC
Expanding agent	–	3% BWOC
Silica flour	35% BWOC	35% BWOC

BWOC, by weight of cement.

Table 2—Design recipes for the small-scale mixing of Class G cement paste and medium-scale batch mixing of expanding Class G cement paste.

Testing Protocols. ***Rheometer and Viscometer Measurements.*** A scientific rheometer (Anton Paar MCR301) was used for accurate characterization of the calibration fluids listed in **Table 1**. Fluid characterization was performed according to the following measurement sequence using the CP75 cone and plate geometry: (i) 2 minutes preshear at fixed shear rate of 1,100 s^{-1}; (ii) logarithmic decrease of shear rate from 1,000 s^{-1} to 10^{-5} s^{-1}; (iii) logarithmic increase of shear rate up to 1,000 s^{-1}. The measurement point duration was fixed at 2 seconds.

An oilfield standard Fann 35 viscometer with the R1-B1 Couette geometry was used for independent viscosity measurements of all hardening fluids in **Table 1**. The procedure defined in the API 10B-2 standard (*API 10B-2* 2013) was adopted (i.e., acquiring the stator dial reading following 10 seconds of shearing at each consecutive rotational speed). Readings were taken at constant rotational speeds ranging from 0.9 rev/min up to 300 rev/min. From 300 rev/min, the measurement sequence is repeated down to 0.9 rev/min, for the purpose of identifying a possible thixotropic fluid response (Nelson and Guillot 2006). Non-Newtonian end effect and shear rate corrections (Lac and Parry 2017; Skadsem and Saasen 2019) were applied when converting revolutions per minute and dial reading to corresponding shear rate and shear stress, respectively.

Pipe Viscometer. Fluid rheograms were obtained from the pipe viscometer by measuring the differential pressure over a section of a horizontal pipe while imposing a volumetric flow rate using a positive displacement pump. The conversion of flow rate and differential pressure (wall shear stress) to equivalent wall shear rate was performed as described in the pipe viscometer design section. To cover relevant wall shear rates in the pipe viscometer, the imposed flow rate was varied from a maximum of approximately 40 L/min (10.6 gal/min) to a minimum flow rate of approximately 3 L/min (0.8 gal/min). **Fig. 3** presents the initial tests involving five different procedures for controlling the imposed flow rate: (i) continuous ramping from maximum to minimum flow rate over a duration of 180 seconds; (ii) discrete flow rate variation with a step of 1.7 L/min (0.4 gal/min) and a continuous measurement duration of 5 seconds per flow rate [ΔQ = 1.7 L/min (0.4 gal/min), Δt = 5 seconds]; (iii) ΔQ = 0.85 L/min (0.2 gal/min), Δt = 5 seconds; (iv) ΔQ = 1.7 L/min (0.4 gal/min), Δt = 10 seconds; (v) ΔQ = 0.85 L/min (0.2 gal/min), Δt = 10 seconds. Initial testing using calibration fluids suggested little or no sensitivity to the different procedures. Consequently, the results presented in this study are all based on continuous ramping of the positive displacement pump output (i).

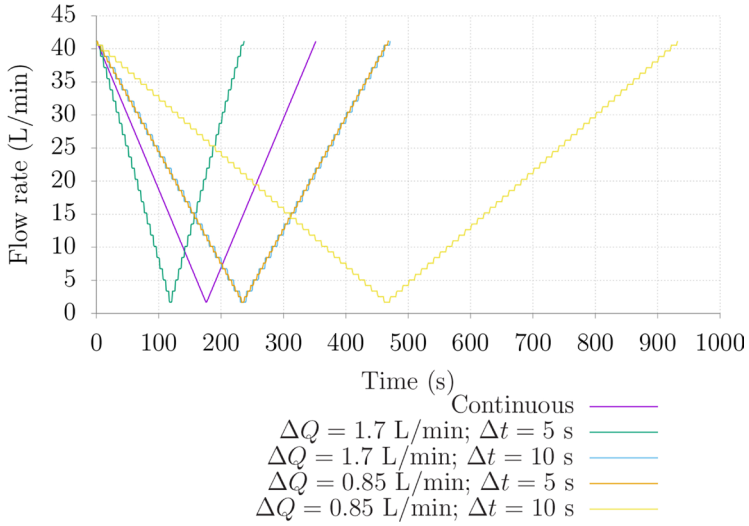

Fig. 3—Test procedures tested using the pipe viscometer setup.

Results and Discussions

In the following sections, flow curves obtained with the pipe viscometer are compared to the independent viscosity characterization using a rheometer or oilfield viscometer. Results are first presented for the calibration fluids, followed by small-scale batch mixes of

conventional Class G oilwell cement paste and three alternative barrier materials. We end the section by discussing medium-scale mixing of expanding Class G oilwell cement and the associated pipe viscometer results.

Calibration Fluids. Measurements of the friction pressure gradient, $\Delta p/\Delta L$, for the calibration fluids glycerol and xanthan gum solution are shown in **Fig. 4a.** Glycerol exhibits a linear relationship between the imposed flow rate and the corresponding friction pressure gradient, as expected for the fully developed, laminar flow of Newtonian fluids. The xanthan gum solution exhibits a nonlinear trend that is consistent with shear-thinning behavior (i.e., the friction pressure gradient increase in response to a flow rate increment is less at higher flow rates). Shown in **Fig. 4b** are the corresponding wall shear rates for the two calibration fluids, as obtained by evaluating Eq. 1. The vertical axis in the figure corresponds to the Newtonian wall shear rate (i.e., $\dot{\gamma}_{wN} = 8\bar{u}/D$). We note that Eq. 1 reproduces the Newtonian result to a very good approximation for glycerol, as expected. For the shear-thinning xanthan gum solution on the other hand, the actual wall shear rate $\dot{\gamma}_w$ is significantly larger than the Newtonian value across the entire measurement interval. This is also to be expected because a shear-thinning (power law) viscosity function results in a larger shear rate close to the wall, as reflected in the fully developed velocity profile for such fluids in pipes (Bird et al. 1987).

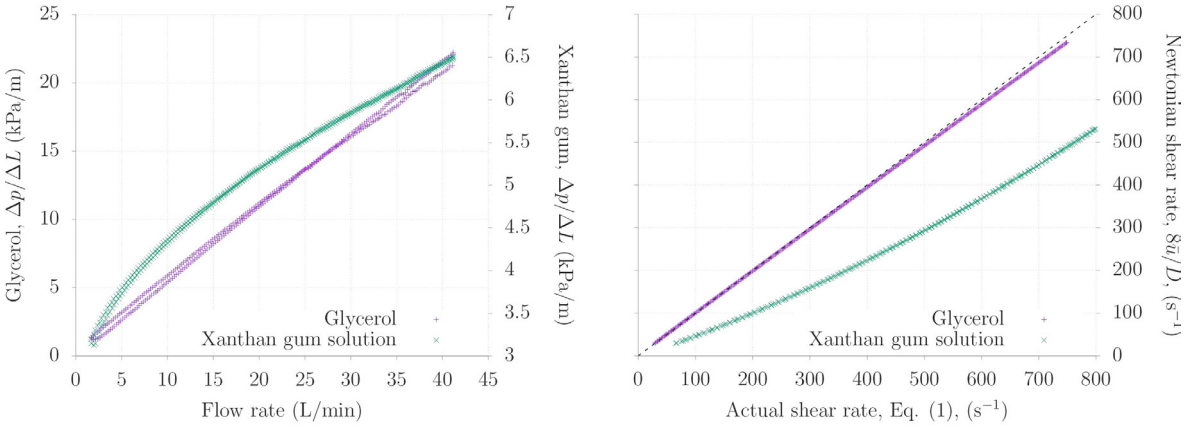

(a) Measured friction pressure gradient as a function of imposed flow rate.

(b) Comparison of wall shear rates.

Fig. 4—Measurements using glycerol and a xanthan gum solution as Newtonian and non-Newtonian (shear-thinning) test fluids. The pipe viscometer is operated by imposing a known volumetric flow rate while measuring the differential pressure drop over a pipe segment. The corresponding friction pressure gradients for flow rates ranging from about 2 L/min (0.5 gal/min) to approximately 40 L/min (10.6 gal/min) are shown in (a). In (b), we compare the actual wall shear rate, from Eq. 1, to the Newtonian wall shear rate, $8\bar{u}/D$.

Armed with the appropriate wall shear rates, $\dot{\gamma}_w$, we may next convert the measurements of friction pressure gradient and imposed flow rate in **Fig. 4a** to flow curves (i.e., plots of wall shear stress as a function of actual wall shear rates). The equivalent results for glycerol and the xanthan gum solution are shown in **Figs. 5a and 5b.** Also shown in the figures as filled circles are the corresponding flow curves acquired from the independent rheometer measurements. The curves represent Newtonian or Herschel-Bulkley parametrization; for the latter, measurements of wall shear stress and wall shear rate are fitted according to $\tau_w = \tau_y + K\dot{\gamma}_w^n$, with τ_y, K, and n being the yield stress, the consistency index, and the flow index in the Herschel-Bulkley model, respectively.

We observe in **Fig. 5a** an excellent agreement between the flow curves produced by the pipe viscometer and the rheometer for glycerol. The two independent measurements are in quantitative agreement and suggest a constant viscosity of 0.157 Pa·s (157 cp). The independent measurements for the xanthan gum solution shown in **Fig. 5b** are also in very good agreement across the shear rate interval where they overlap. Although the resulting model parameters acquired from the pipe viscometer and the rheometer are different, the two measurement methods are considered to be in excellent agreement within the overlapping measurement interval (i.e., for wall shear rates larger than approximately 100 s^{-1}). We note that the considerable degree of shear-thinning exhibited by this polymeric liquid ($n \approx 0.33$ according to the rheometer data) as well as the available flow rate interval in the pipe viscometer limited our ability to characterize the low-end shear rate region of this fluid. We also note that for high shear rates, the flow of the xanthan gum solution was likely not fully developed at the beginning of the measurement section; the measurement points in question are indicated by gray point coloring in **Fig. 5b**. For the xanthan gum solution, the relatively low effective viscosity caused high Reynolds numbers at the highest imposed flow rates and a violation of the development flow criterion. As such, the points likely corresponding to only partly developed flow have not been included in the viscosity parametrization, which was determined to be $\tau = (13.85 + 0.16\dot{\gamma}^{0.70})$ Pa for the pipe viscometer measurements.

Finally, the comparison between the Coriolis density measurement and the corresponding density inferred from pressure measurements taken in the horizontal and vertical pipes is shown in **Fig. 6** for the xanthan gum solution. One can note a maximum difference of up to 7% when comparing the two measurements. The density reading provided by the Coriolis flowmeter appeared very stable at all flow rates, while measurements using the pipe system exhibited larger fluctuations, probably linked to pressure variations or inaccurate pressure recordings. Based on the observations made in the current study, pressure-based density estimation is considered a viable option whenever a Coriolis flowmeter or a similar density meter is not available. However, as seen in **Fig. 6**, we found the flowmeter to output a more stable and accurate density value. In what follows, we use the density measurement as reported by the Coriolis flowmeter for fluid characterization.

Small-Scale Batch Mixing Tests. Portland cement paste, generally Class G or H, is the material most commonly used in primary and remedial cementing jobs. However, there are currently several types of new materials, ranging from considering cement clinker additions to new formulations with different precursor and activator materials. Therefore, the results of the flow curves will be presented below in two subsections, considering the Class G cement paste and a second subsection with the alternative materials chosen for the study,

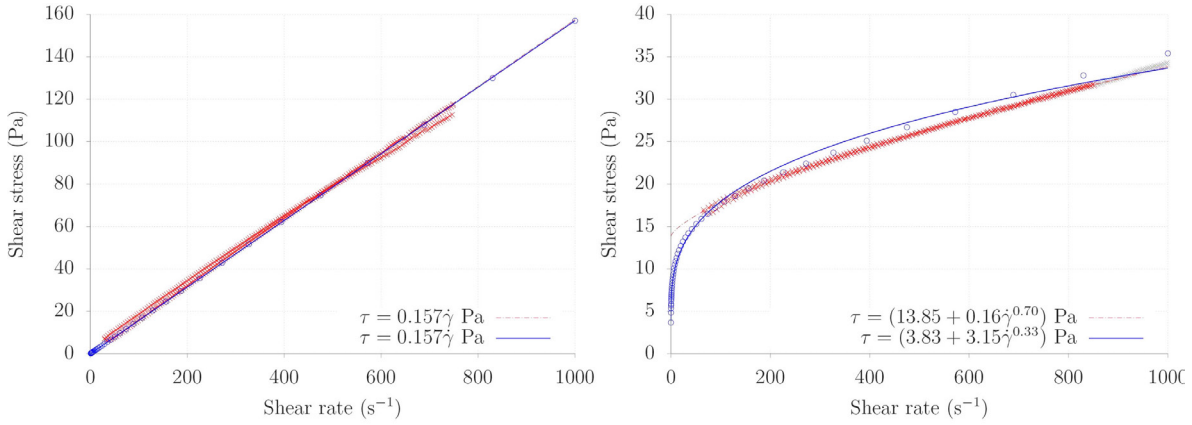

(a) Glycerol.

(b) Xanthan gum solution.

Fig. 5—Flow curve measurements using the Anton Paar rheometer (circles and solid curve) and pipe flow loop viscometer (dense points and dashed curve) for the two calibration fluids. As explained in the text and indicated by the gray measurement point coloring in the figure, high shear rate pipe viscometer measurements of xanthan gum solution were in violation of the development length criterion. As such, these measurements were not included in the viscosity parametrization shown in the figure.

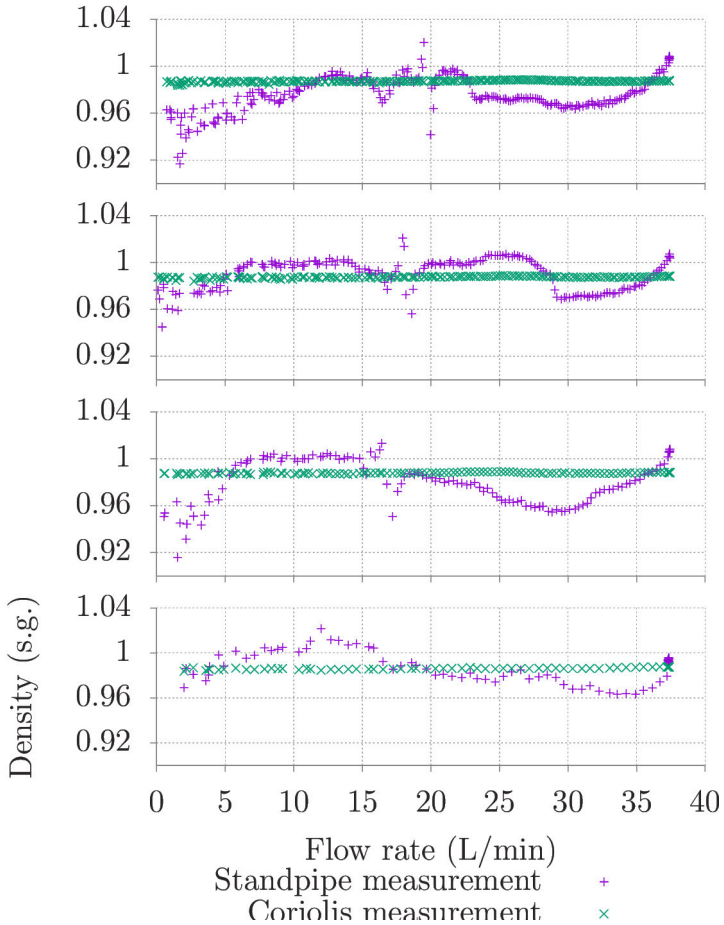

Fig. 6—Comparison of fluid mass density as measured using the instrumented standpipe principle and the Coriolis flowmeter.

utilizing a small-scale mixing tank [50 L (13.2 gal)]. **Table 1** presents these materials with properties that can help explain the rheological results obtained.

Class G Cement Paste. **Fig. 7** presents the flow curves for the measurements performed in the conventional Class G cement paste at four different points in time, using the pipe viscometer and the Couette (Fann 35) viscometer. In **Fig. 7**, the filled symbols refer to Couette viscometer measurements, the continuous line is its Herschel-Bulkley model, the crosses refer to pipe flow measurements, following the Mooney-Rabinowitsch relation, and the dashed-dotted line is its Herschel-Bulkley model.

We find that both sets of measurements can be fitted well using the Herschel-Bulkley model, as expected. However, we also observe that the measurements taken with the Couette viscometer suggested a higher effective viscosity compared to the pipe viscometer. This

trend is seen for all shear rates in **Fig. 7a**. Shown in **Fig. 7b** are repeat measurements of the flow curve, taken at later times since adding dry ingredients to the batch mixer. Also in the repeat measurements, we observe a similar difference between Couette and pipe viscometer measurements, where Couette measurements yield a larger shear stress and effective viscosity than the pipe viscometer. As measurements on the particle-free calibration fluids produced excellent agreement between the Couette and the pipe viscometer **(Fig. 5)**, the differences between the viscometers observed in **Fig. 7** may be linked to the effects of cement particles on the measurements. Possible mechanisms that may contribute to differences between the flow curves include the following: (i) A delay between fluid sampling and taking the Couette measurements, which may result in some viscosification and/or cooling of the sample; (ii) particle migration and apparent wall slip in the pipe viscometer, resulting in a reduction in the measured friction pressure; and (iii) nonuniform properties of the cement paste, resulting in different properties between the fluid sampled for Couette measurements and that flowing through the pipe.

Finally, we note that the successive flow curves measured at later times since the start of mixing show a trend toward lower effective viscosity (i.e., reduced shear stress at a given shear rate). We attribute this observation to the heating of the paste as it is recirculated through the batch mixer; a temperature increase of approximately 4.5°C (8.1°F) was recorded during the measurement sequence.

Alternative Barrier Materials. **Fig. 8** presents flow curves for the three alternative barrier materials tested using the pipe viscometer. As above, filled symbols refer to Couette viscometer (Fann 35) measurements, and the continuous line is its Herschel-Bulkley model, while crosses refer to pipe flow measurements, following the Mooney-Rabinowitsch relation, and the dashed-dotted line is its Herschel-Bulkley model. For the self-healing cement paste and geopolymer paste in particular, pipe viscometer measurements at greater flow rates (i.e., shear rates) resulted in generalized Reynolds numbers that were incompatible with the entrance length criterion corresponding to fully developed laminar flow at the start of the measurement section. These intervals of the flow curves are indicated by gray marker color and have not been used in the Herschel-Bulkley parametrization of the pipe viscometer flow curves. In the case of **Fig. 8b**, we note an apparent shear-thickening behavior at the largest wall shear rates; we attribute this trend to incomplete flow development, causing a larger friction pressure gradient than that corresponding to fully developed flow (White 1991).

In shear rate regions where the pipe viscometer and the Couette viscometer overlap, we find comparable levels of shear stress and effective viscosity values that are in good quantitative agreement. Measurements acquired with the two viscometers are found to be in better agreement for the three alternative barrier materials than for the conventional Class G cement paste, as shown in **Fig. 7a**. The improved quantitative agreement observed in **Fig. 8** suggests either more consistent fluid sampling and characterization procedures, improved mixing of the slurries (i.e., more uniform fluids), and/or minor or negligible impact of wall slip in the pipe viscometer.

While the flow curve measurements from the Couette and pipe viscometers are generally in good agreement across the overlapping shear rate regions, we note that the measurements result in different Herschel-Bulkley parametrizations, as indicated in the legends to **Fig. 8**. We attribute the different parametrizations mainly to the lack of low-shear rate measurements in the pipe viscometer; as a consequence of not sampling the lower shear rates, the shear-thinning behaviors of the self-healing cement paste and the geopolymer paste are not captured. Consequently, the pipe viscometer flow curves are better approximated by the two-parameter Bingham plastic model, which results in an overestimation of the low-shear rate effective viscosity as well as the yield stress behavior of these slurries. A similar trend of larger pipe viscometer yield stress values compared to Couette measurements has been found by, for example, Shah and Sutton (1990). Improved resolution of the low-shear rate flow curves can be achieved by reducing the minimum imposed flow rate and/or adding a second measurement section with a larger inner diameter than the current section.

Fig. 9 shows the evolution of the flow curves over time for each alternative material tested. As above, the time indicated in the figure legends corresponds to the time since adding dry ingredients to the batch mixer. While both the corrosion-resistant and the self-healing cement pastes allowed characterization for over at least 62 minutes since adding dry ingredients, the geopolymer paste exhibited significant deviations in the friction pressure measurements and gelation in the Couette viscometer during the third and fourth measurement sequences. As such, only two successive measurement series are shown in **Fig. 9c**. The repeat measurements shown in **Fig. 9** are generally found to be consistent with the initial observations in **Fig. 8** (i.e., satisfactory quantitative agreement between Couette and pipe viscometer measurements across the overlapping shear rate regions).

From **Fig. 10,** it is possible to compare the pump power and temperature variation over time for the alternative materials tested. In the case of the geopolymer paste, it is possible to notice the tendency to reduce pump power and increase the fluid temperature even with only two measurements, presenting similar behavior to that observed for the other two materials. However, the gelation and set processes for subsequent measurements impacted the pump power measurement, with an increase in energy consumed from the third measurement onward and, consequently, a considerable increase in the paste temperature. This behavior indicates that the transition from the liquid to the solid phase has already started. This statement can be supported by data from the thickening time test, where the fluid takes about

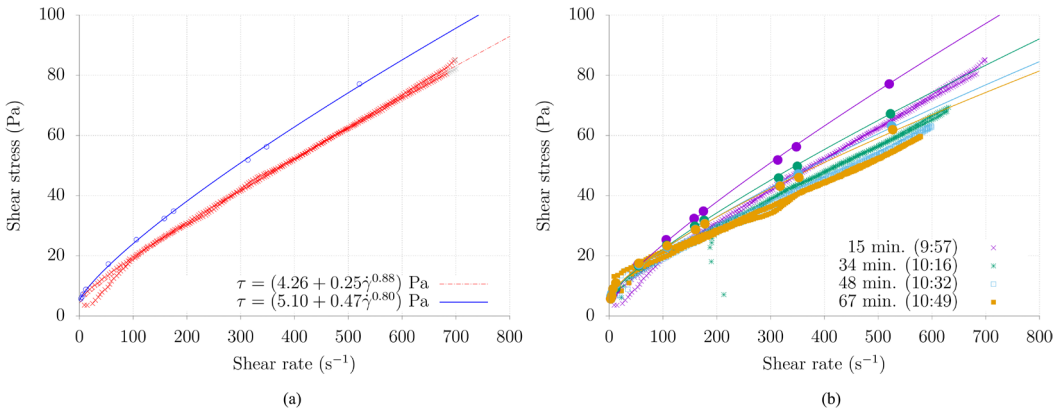

Fig. 7—Flow curve measurements for the conventional Class G cement pastes tested using a 50-L mix tank, where (a) presents the cement Class G first measurement and (b) the evolution of the flow curve considering four measurements. Solid circles correspond to Couette (Fann 35) viscometer measurements, and the densely positioned measurement points are from the pipe viscometer. The legend in (b) identifies the time since adding the dry ingredients to the batch mixer and the corresponding time of day (in parentheses).

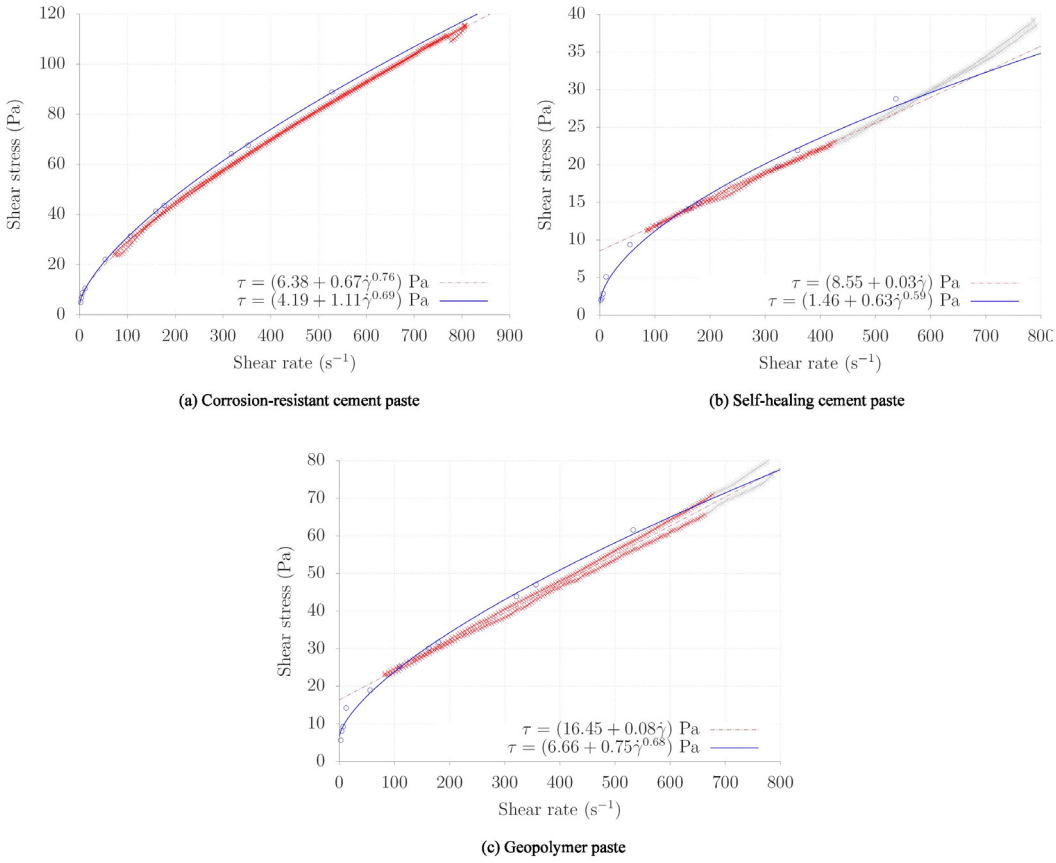

Fig. 8—Flow curve measurements for the alternative barrier materials tested, comparing Couette viscometer measurements (filled circles) to pipe viscometer measurements (crosses). The pipe viscometer measurements marked by gray color in (b) and (c) correspond to conditions where the flow was likely not fully developed at the entrance to the measurement sections. These points have not been included in the corresponding flow curve parametrization.

50 minutes to reach the point of departure and approximately 5 hours to reach 100 Bearden consistency units, considering a test temperature of 30°C (86°F) and a test pressure of 35 bar (507.5 psi).

Medium-Scale Mixing Test and Fluid Characterization. The final test included in this study represented the mixing and characterization of a larger volume of expanding Class G oilwell cement, mixed using a specially designed in-house batch mixer. The design of the batch mixer is based on equivalent field-scale recirculation mixers but is constructed with the intention of effectively mixing smaller volumes of cement paste [up to 600 L (158.4 gal)] mainly for research and testing purposes. A schematic of the batch mixer and the interfaced pipe viscosmeter is provided in **Fig. 11.** We point out that the medium-scale mixing unit is operated as a batch mixer, which means that relatively small volumes [≤600 L (158.4 gal)] can be prepared at the time. As a consequence, the pipe viscometer is installed and operated in parallel to the main recirculation line. An alternative field implementation suitable for continuous ("on-the-fly") cement paste mixing can be to integrate the pipe viscometer in parallel to lines that feed cement paste to the rig displacement pump(s) and, as such, measure the properties of the paste as it is pumped downhole. Such an installation may even enable characterization of *all* cementing fluids pumped downhole, not just of the cement paste/barrier fluid.

Returning to the medium-scale mixer in **Fig. 11**, the main mixing action is provided by the centrifugal pump that ensures recirculation of the paste contained in the tank. The pump is fed through a drain at the bottom of the tank, and the paste is circulated back to the tank through a hopper arrangement. To compensate for the lack of an internal paddle in the mixing tank, the paste is conditioned by recirculating at a reduced rate before cementing. As shown in the schematic, the pipe viscometer was fitted into the existing batch mixer by having a suction line before the centrifugal pump on the recirculation line, with a return either directly downstream of the centrifugal pump or through a dedicated line back to the mixing tank. Also shown in the schematic is a disposal tank for surplus paste and liquids, as well as casing test sections that were to be cemented by the mixed cement paste. These test sections were cemented for a separate project and for the purpose of measuring the gas permeability of full-scale diameter cement plugs inside casings.

The medium-scale mixing unit was equipped with instrumentation to record the density of the paste being mixed, the weight of the mixing tank, and the temperature of the fluid contained inside the tank, as well as the flow rate at which paste was being recirculated through the mixing tank. In **Fig. 12,** a temporal diagram is provided that shows how these variables evolved over the course of the cement paste mixing period.

The batch mixer was initially filled with the design volume of the mixing water, and mixing commenced at approximately 09:30 by starting the recirculation pump and gradually adding dry ingredients through the hopper. This phase lasted until approximately 10:00, at which time the target paste density was reached (1.92 s.g.). We note a constant temperature increase throughout this phase of the mixing, mostly attributed to the action of the centrifugal pump that circulated the paste through the batch mixer at a flow rate close to 3000 L/min (792 gal/min). From approximately 10:05 and onward for about 40 minutes, paste conditioning took place. The pump operated at about 50% capacity, and the paste temperature stabilized above 30°C (86°F). Starting at about 10:48, the mixed cement paste was pumped toward the two casing test sections, resulting in gradual reductions in the batch mixer tank weight.

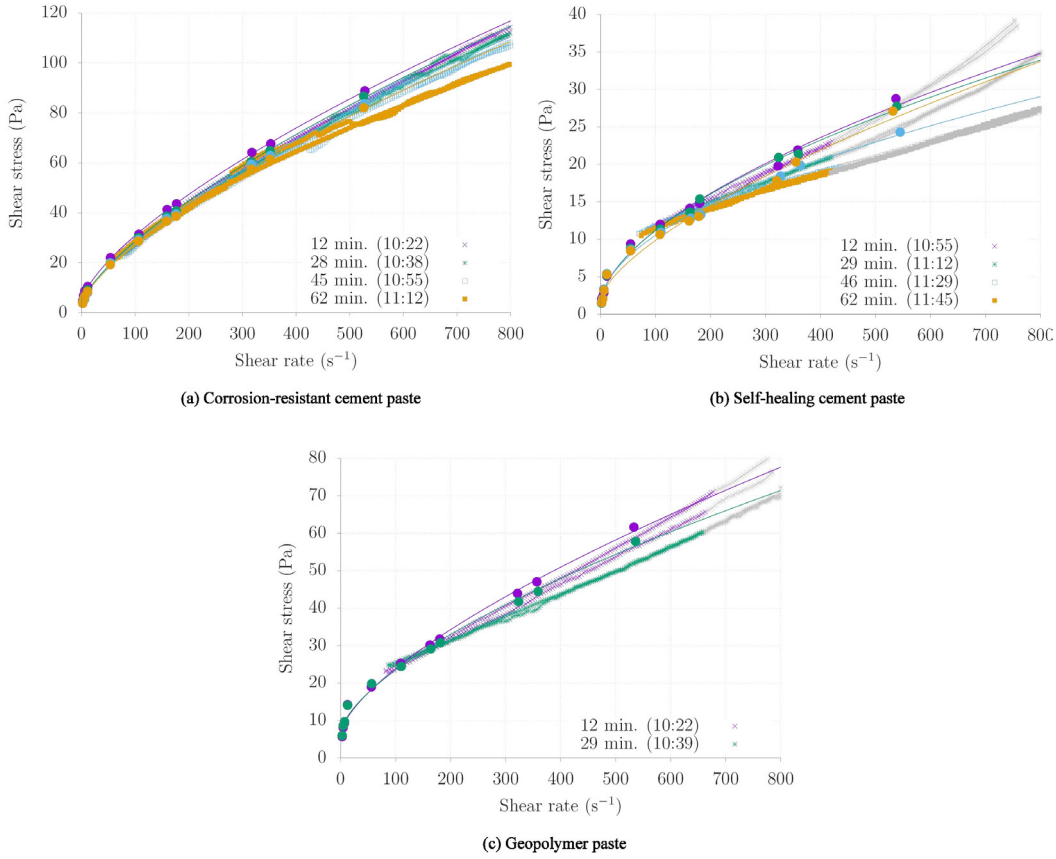

Fig. 9—Evolution of the flow curve measurements for the alternative barrier materials tested, comparing Couette viscometer measurements (filled circles) to pipe viscometer measurements (crosses). The legends in the figures identify the time since adding the dry ingredients to the batch mixer and the corresponding time of day (in parentheses).

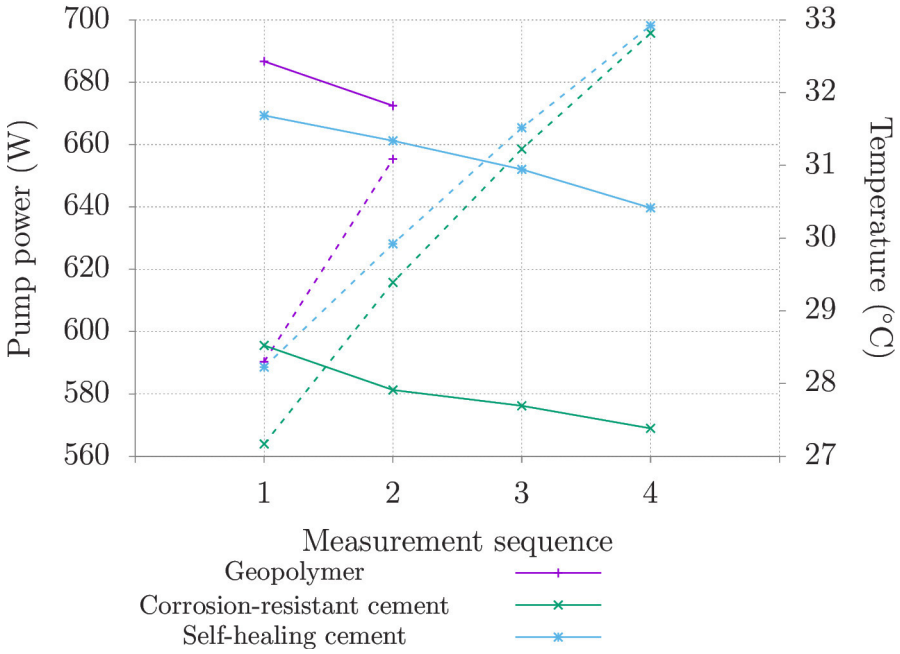

Fig. 10—Pump power and temperature variations through the viscosity tests performed using the pipe viscometer system. Measurements represented by solid curves correspond to pump power, while dashed curves represent temperature measurements.

At three instances during the medium-scale mixing, cement paste was passed to the pipe viscometer, which was connected in parallel to the recirculation line, as shown in **Fig. 11**. Samples were acquired at 10:15 (early stage of conditioning phase), 10:37 (late stage of conditioning phase), and 11:06 (at the end of the cementing operation).

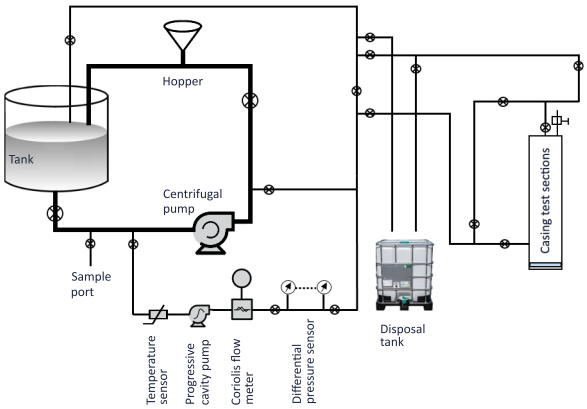

Fig. 11—Schematic showing the interface between the pipe viscometer and the medium-scale batch mixing unit.

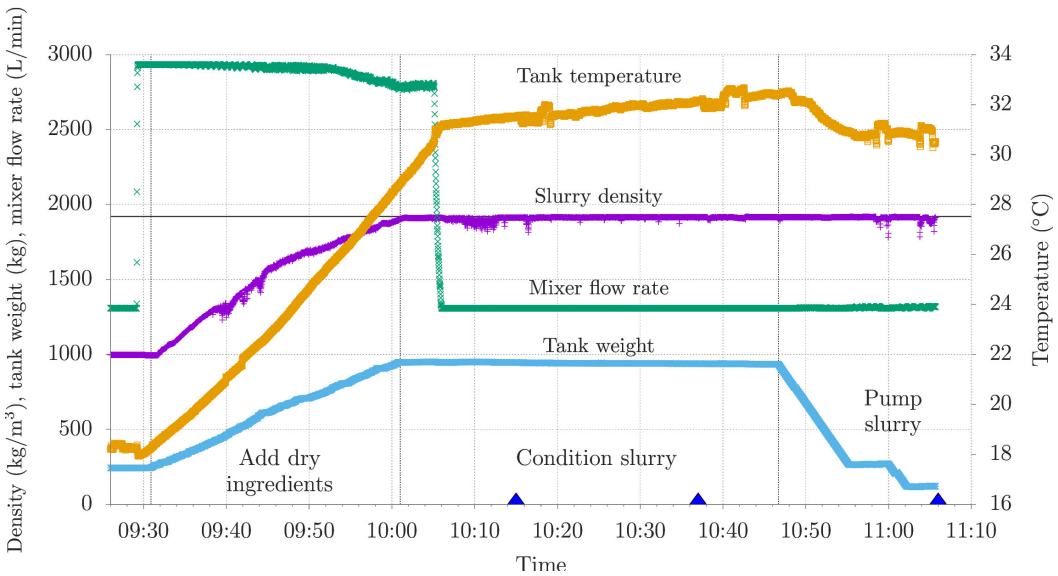

Fig. 12—Measurements acquired during medium-scale batch mixing of an expanding cement paste. The target density was 1920 kg/m^3 (16.02 lbm/gal), as indicated by the horizontal line. The paste mixing procedure comprised the addition of dry ingredients at the maximum recirculation flow rate through the mixer (up until about 10:00), followed by conditioning at an intermediate recirculation rate (up until about 10:48), and finally paste placement in prepared full-scale casing test sections. Samples of expanding cement paste were characterized in the pipe viscometer at 10:15, 10:37, and 11:06, indicated by the triangle symbols along the horizontal axis in the figure.

Shown in **Fig. 13** are the flow curves acquired from the pipe viscometer and using the Couette viscometer (Fann 35) at different times during the conditioning and cementing stages of the operation. The time intervals indicated in the legend of the figure correspond to the time at which all dry ingredients were added to the mixer and the time at which the fluid sample was acquired for characterization. Couette viscometer flow curves are included only for the first two sampling times; the final sample acquired for Couette viscometer measurement exhibited significantly reduced effective viscosity. We attribute this response to either unintentional dilution or an inhomogeneous fluid sample that is not representative of the paste behavior. This sample is therefore not included in the figure.

As per previous tests on a smaller scale, we find a satisfactory agreement between pipe viscometer measurements and the corresponding Couette viscometer readings, especially at intermediate and high shear rates. For the first sample, taken 13 minutes after completing the addition of dry ingredients, the pipe viscometer and the Couette viscometer measurements are in excellent agreement at shear rates ranging from 100 s^{-1} and up to approximately 700 s^{-1}. To improve the low-shear rate sampling of the flow curve in the pipe viscometer, the positive displacement pump was operated at very low imposed flow rates. Interestingly, the pipe viscometer–derived flow curves in **Fig. 13** are similar to Bingham plastic models, with no clearly discernible shear-thinning evident at low or intermediate shear rates. The Couette viscometer measurements, which go down to an apparent shear rate of 1.5 s^{-1} clearly suggest shear-thinning.

The next two samples tested in the pipe viscometer, at 35 minutes and 64 minutes after completing the addition of dry ingredients, show similar behavior and a slightly greater effective viscosity than the first measurement. The temperature in the mixing tank was nearly constant throughout the conditioning phase, so the slight increase in effective viscosity may be attributed to the maturing or conditioning of the paste. The Couette viscometer measurements performed after 35 minutes also indicate an increased effective viscosity compared to the first measurement, consistent with the pipe viscometer measurements. The observed difference between pipe viscometer and Couette viscometer flow curves may be attributed to uncertainty in the wall shear rate estimation at low imposed flow rates (Magnon and Cayeux

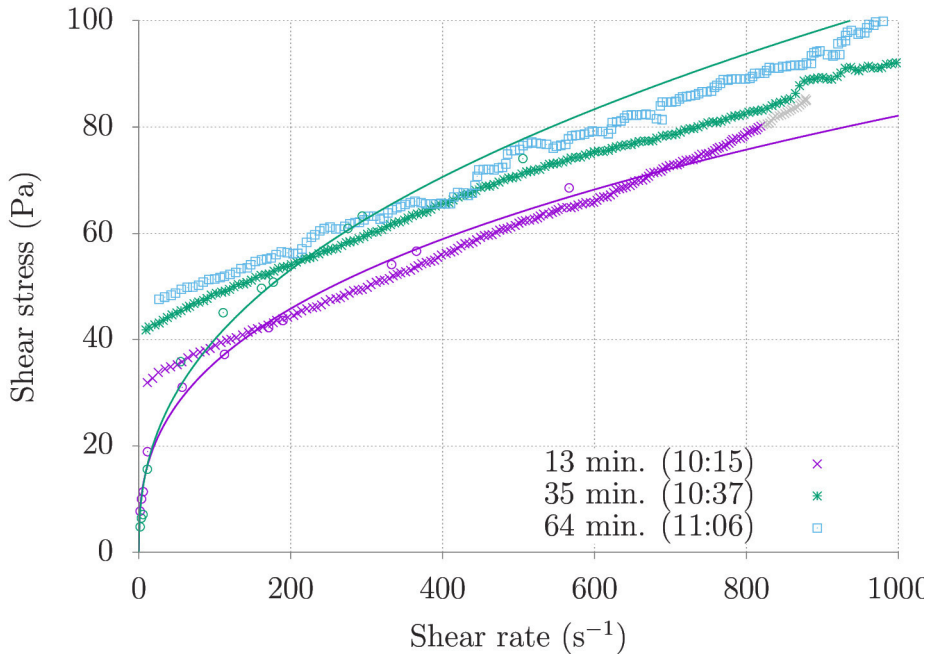

Fig. 13—Flow curve measurements for samples acquired during medium-scale [550 L (145 gal)] mixing of expanding Class G cement pastes tested using a 600-L (158 gal) mixing tank. The legend identifies the time since adding the dry ingredients to the batch mixer and the corresponding time of day (in parentheses).

2021). Possible improvements to the processing of viscometer measurements, or indeed the pump operation during the measurement sequence, will be considered in future developments of the pipe viscometer.

Current Study Limitations and Uncertainty. The current pipe viscometer design uses a single pipe diameter—D = 0.0212 m (0.835 in)—for the measurement section, and this impacts the current capabilities of the pipe viscometer in two main ways: First and as seen from the flow curve for the low-viscosity self-healing cement paste **(Fig. 7b)**, the combination of pipe diameter, fluid properties, and entrance length of the pipe limits the availability of shear rate interval for fluid characterization. Further and as seen from **Figs. 5b and 8**, several flow curves terminate at the lowest shear rate of approximately 100 s^{-1} at the selected minimum imposed flow rate. In either case, the limited shear rate interval available for observation impacts the determination of constitutive model parameters, such as the yield stress and/or the flow index, which are connected to shear-thinning behavior and are most readily observed at low to intermediate shear rates. Examples where we find reasonably good agreement with the independent viscometer/rheometer characterization include the xanthan gum solution, **Fig. 4b**, and the corrosion-resistant cement paste, **Fig. 7a**. For the self-healing cement and geopolymer barrier materials, on the other hand, the estimation of these parameters is less satisfactory. We attribute these differences mainly to the lack of low shear rate observations in the pipe viscometer. Improved estimation of the yield stress parameter can be particularly useful for detailed wellbore flow and fluid displacement analysis, for example, in the determination of displacement along the narrow side of eccentric annuli (Couturier et al. 1990; Walton and Bittleston 1991).

Second, the use of measurement sections with a single pipe diameter prevents the identification of possible wall slip in the pipe. A second, smaller diameter pipe could be included in a revised design of the pipe viscometer to detect and possibly correct for such effects. However, it appears that the current design is capable of providing adequate agreement with independent Couette viscometer measurements for the materials tested in this study.

Summary and Conclusions

The density and viscosity of cementing fluids are carefully designed fluid properties that directly impact downhole mud displacement. Traditional means of measuring these properties in the field include the use of a mud balance and a Couette viscometer. This study presented a pipe viscometer that has been developed to enable future integration into cement mixing units and that allows the simultaneous measurement of both density and fluid viscosity. The pipe viscometer may be interfaced to both smaller volume batch mixing equipment and larger-volume continuous ("on-the-fly") mixing infrastructure and can enable automated and consistent documentation of fluid properties during mixing and/or pumping downhole. The design of the pipe viscometer was made on the basis of the entrance length between the inlet and the measurement section, and consideration of a suitable pipe inner diameter to allow fluid characterization over a wide and relevant range of shear rates. Compared to previous studies, a larger inner pipe diameter is used in the current setup to control possible wall slip effects. The pipe viscometer was designed with two independent means of measuring the fluid density, utilizing a Coriolis flowmeter between the pump and the measurement section and inferring the density from the "standpipe" principle, where the density is obtained from the hydrostatic pressure component measured in a vertical pipe. Our tests showed both approaches to be viable but indicated more stable readings from the Coriolis flowmeter .

Trials with different ramping protocols for the positive displacement pump that feeds test fluid to the pipe and the measurement section suggested that continuous ramping of the flow rate resulted in more stable throughput over the entire measurement interval. A relatively slow ramping rate [varying the flow rate from a maximum of 40 L/min (10.6 gal/min) to a minimum of approximately 3 L/min (0.8 gal/min) over 180 seconds] was defined, thereby preventing time-dependent/thixotropic effects in the test fluid and still enabling a complete ramp within as short a time as possible. Most tests were performed by ramping the flow rate down to the minimum set point, followed immediately by ramping up at the same rate to check for any thixotropic response at the relatively slow time scale of the flow rate ramp. None of the fluids tested in this study exhibited significant thixotropy.

We test the pipe viscometer in this study using conventional and expanding Class G well cements, as well as three alternative well barrier materials. We conclude that the current combination of entrance length, pipe diameter, and imposed flow rate interval is suitable to sample the flow curve over shear rates that are relevant for placement downhole and that overlap with those measured in standard oilfield viscometers. For low-viscosity materials, such as the self-healing cement tested in this study, a longer entrance length or a second, smaller diameter pipe would be required for sampling the upper shear rate range (gt_{450} s^{-1}). The flow curves obtained with the pipe viscometer generally agree with the corresponding Couette viscometer measurements, although the current design and operation of the pipe viscometer limit sampling at the low end of the shear rate interval. Consequently, the flow curve parametrizations result in different values for model parameter values, such as the yield stress. Future work will assess design and operational modifications for extending the shear rate range sampled by the pipe viscometer.

Nomenclature

A = pipe inner cross-sectional area, L^2, m^2
D = pipe inner diameter, L, m
f = Darcy-Weisbach friction factor
K = fluid consistency index, M/LT^{2-n}, $Pa \cdot s^n$
n = flow index
Q = volumetric flow rate, L^3T^{-1}, m^3/s
R = pipe inner radius, L, m
Re_g = generalized Reynolds number
T = temperature, Θ, °C
X_D = development length, L, m
$\dot{\gamma}_a$ = apparent (Newtonian) wall shear rate, T^{-1}, s^{-1}
$\dot{\gamma}_w$ = wall shear rate, T^{-1}, s^{-1}
$\Delta P/\Delta L$ = pressure drop per unit length, M/L^2T^2, Pa/m
μ = viscosity, $ML^{-1}T^{-1}$, Pa·s
ρ = mass density, ML^{-3}, kg/m^3
τ_w = wall shear stress, M/LT^2, Pa
τ_y = yield stress, M/LT^2, Pa
$\bar{u}$ = fluid velocity, L/T, m/s

Acknowledgments

The authors acknowledge the Research Council of Norway (RCN) for financing the Centre for Research–based Innovation *SWIPA-Centre for Subsurface Well Integrity, Plugging and Abandonment*, RCN project number 309646, for which the work has been carried out. The center is also financed by the operating companies AkerBP, Equinor ASA, and Wintershall Dea Norway and includes more than 20 in-kind contributing industry partners. The research and development partners in SWIPA are SINTEF, NORCE, IFE, NTNU, and the University of Stavanger.

The experimental work has been carried out with the use of the research and development infrastructure at *Norwegian P&A Laboratories* (NorPALabs). The authors acknowledge the financial support from RCN for the establishment of the infrastructure (RCN project award no. 296009).

H.J. Skadsem acknowledges Dr. Eric Cayeux, NORCE, for valuable input and stimulating discussions related to the rheological characterization of well construction fluids. Finally, we acknowledge Dave Gardner, NORCE, and the *P&A Innovation Program* for making measurements acquired from the medium-scale batch mixer **(Fig. 12)** available for this study. The Petroleum Safety Authority Norway, AkerBP, ConocoPhillips, Petrobras, Shell, and TotalEnergies are partners in the *P&A Innovation Program,* a program for accelerating plugging and abandonment technology development.

References

API 10B-2, *Recommended Practice For Testing Well Cements*. 2013. Washington, D.C: American Petroleum Institute.

Bannister, C. E. 1980a. Rheological Evaluation Of Cement Slurries: Methods And Models. Paper presented at the SPE Annual Technical Conference and Exhibition, Dallas, Texas, USA, 21–24 September. SPE-9284-MS. https://doi.org/10.2118/9284-MS.

Bannister, C. E. 1980b. Rheological Evaluation Of Cement Slurries: Methods And Models. Paper presented at the SPE Annual Technical Conference and Exhibition, Dallas, Texas, USA, 21–24 September. SPE-9284-MS. https://doi.org/10.2118/9284-MS.

Bannister, C. E. and Benge, O. G. 1981. Pipe Flow Rheometry: Rheological Analysis Of A Turbulent Flow System Used For Cement Placement. Paper presented at the SPE Annual Technical Conference and Exhibition, San Antonio, Texas, USA, 4–7 October. SPE-10216-MS. https://doi.org/10.2118/10216-MS.

Bird, R. B., Armstrong, R. C., and Hassager, O. 1987. *Dynamics of Polymeric Liquids*. Hoboken, New Jersey, USA: John Wiley & Sons, Inc.

Carlsen, L. A., Rolland, N. L., Nygaard, G. et al. 2013. Simultaneous Continuous Monitoring of the Drilling-Fluid Friction Factor and Density. *SPE Drill & Compl* **28** (1): 34–44. SPE-163101-PA. https://doi.org/10.2118/163101-PA.

Carrasco-Teja, M., Frigaard, I. A., Seymour, B. R. et al. 2008. Viscoplastic Fluid Displacements in Horizontal Narrow Eccentric Annuli: Stratification and Travelling Wave Solutions. *J Fluid Mech* **605**: 293–327. https://doi.org/10.1017/S0022112008001535.

Cayeux, E. 2020. Time, Pressure and Temperature Dependent Rheological Properties of Drilling Fluids and Their Automatic Measurements. Paper presented at the IADC/SPE International Drilling Conference and Exhibition, Galveston, Texas, USA, 3–5 March. SPE-199641-MS. https://doi.org/10.2118/199641-MS.

Cayeux, E. and Leulseged, A. 2020. The Effect of Thixotropy on Pressure Losses in a Pipe. *Energies* **13** (23): 6165. https://doi.org/10.3390/en13236165.

Clark, P. E. and Shaughnessy, R. J. 1990. Rheological Evaluation of Dense Suspensions: Simulation of a Fresh Cement Paste. *SPE Prod Eng* **5** (2): 180–186. SPE-18526-PA. https://doi.org/10.2118/18526-PA.

Couturier, M., Guillot, D., Hendriks, H. et al. 1990. Design Rules And Associated Spacer Properties For Optimal Mud Removal In Eccentric Annuli. Paper presented at the CIM/SPE International Technical Meeting, Calgary, Alberta, Canada, 10–13 June. SPE-21594-MS. https://doi.org/10.2118/21594-MS.

Gul, S., Erge, O., and van Oort, E. 2020a. Helical Pipe Viscometer System for Automated Mud Rheology Measurements. Paper presented at the IADC/SPE International Drilling Conference and Exhibition, Galveston, Texas, USA, 3–5 March. SPE-199572-MS. https://doi.org/10.2118/199572-MS.

Gul, S., Erge, O., and van Oort, E. 2020b. Frictional Pressure Losses of Non-Newtonian Fluids in Helical Pipes: Applications for Automated Rheology Measurements. *J Nat Gas Sci Eng* **73**: 103042. https://doi.org/10.1016/j.jngse.2019.103042.

Gul, S., Oort, E., Mullin, C. et al. 2020c. Automated Surface Measurements of Drilling Fluid Properties: Field Application in the Permian Basin. Paper presented at the SPE/AAPG/SEG Unconventional Resources Technology Conference, . , , Denver, Colorado, USA, 22–24 July. URTEC-2019-964-MS. https://doi.org/10.15530/urtec-2019-964.

Lac, É. and Parry, A. 2017. Non-Newtonian End-Effects in Standard Oilfield Rheometers. *J of Rheol* **61** (4): 833–843. https://doi.org/10.1122/1.4986925.

Liu, N., Gao, H., Xu, Y. et al. 2022. Design and Use of an Online Drilling Fluid Pipe Viscometer. *Flow Meas Instrum* **87**: 102224. https://doi.org/10.1016/j.flowmeasinst.2022.102224.

Magnon, E. and Cayeux, E. 2021. Precise Method to Estimate the Herschel-Bulkley Parameters from Pipe Rheometer Measurements. *Fluids* **6** (4): 157. https://doi.org/10.3390/fluids6040157.

Mannheimer, R. J. 1991. Laminar and Turbulent Flow of Cement Slurries in Large Diameter Pipe: A Comparison with Laboratory Viscometers. *J of Rheol* **35** (1): 113–133. https://doi.org/10.1122/1.550223.

Nelson, E. and Guillot, D. 2006. *Well Cementing*. Houston, Texas, USA: Schlumberger.

Ofoche, P. and Noynaert, S. 2020. Real-Time Measurement of Drilling Fluid Rheology and Density Using Acoustics. Paper presented at the Abu Dhabi International Petroleum Exhibition & Conference, Abu Dhabi, UAE, 9–12 November. SPE-203389-MS. https://doi.org/10.2118/203389-MS.

Pelipenko, S. and Frigaard, I. A. 2004. Visco-Plastic Fluid Displacements in near-Vertical Narrow Eccentric Annuli: Prediction of Travelling-Wave Solutions and Interfacial Instability. *J Fluid Mech* **520**: 343–377. https://doi.org/10.1017/S0022112004001752.

Poole, R. J. and Chhabra, R. P. 2010. Development Length Requirements for Fully Developed Laminar Pipe Flow of Yield Stress Fluids. *J Fluids Eng* **132** (3). https://doi.org/10.1115/1.4001079.

Poole, R. J. and Ridley, B. S. 2007. Development-Length Requirements for Fully Developed Laminar Pipe Flow of Inelastic Non-Newtonian Liquids. *J Fluids Eng* **129** (10): 1281–1287. https://doi.org/10.1115/1.2776969.

Press, W. H., Teukolsky, S. A., Vetterling, W. T. et al. 2001. *Numerical Recipes in Fortran 77*, second edition. Cambridge, UK: Cambridge University Press.

Rabinowitsch, B. 1929. Über Die Viskosität Und Elastizität von Solen. *Zeitschrift Für Physikalische Chemie* **145A** (1): 1–26. https://doi.org/10.1515/zpch-1929-14502.

Shah, S. N. and Sutton, D. L. 1990. New Friction Correlation for Cements From Pipe and Rotational-Viscometer Data. *SPE Prod Eng* **5** (4): 415–424. SPE-19539-PA. https://doi.org/10.2118/19539-PA.

Skadsem, H. J. and Saasen, A. 2019. Concentric Cylinder Viscometer Flows of Herschel-Bulkley Fluids. *Appl Rheol* **29** (1): 173–181. https://doi.org/10.1515/arh-2019-0015.

Sui, D. and Vidaur, J. C. M. 2020. Automated Characterization of Non-Newtonian Fluids Using Laboratory Setup. *Appl Rheol* **30** (1): 39–53. https://doi.org/10.1515/arh-2020-0101.

Taugbøl, K., Sola, B., Forshaw, M. et al. 2021. Automatic Drilling Fluids Monitoring. Paper presented at the SPE/IADC International Drilling Conference and Exhibition, Virtual, 8–12 March. SPE-204041-MS. https://doi.org/10.2118/204041-MS.

Théron, B. E., Bodin, D., and Fleming, J. 2002. Optimization of Spacer Rheology Using Neural Network Technology. Paper presented at the IADC/SPE Drilling Conference, Dallas, Texas, USA, 26–28 February. SPE-74498-MS. https://doi.org/10.2118/74498-MS.

Walton, I. C. and Bittleston, S. H. 1991. The Axial Flow of a Bingham Plastic in a Narrow Eccentric Annulus. *J Fluid Mech* **222** (1): 39. https://doi.org/10.1017/S002211209100099X.

White, F. M. 1991. *Viscous Fluid Flow*, second edition. New York, New York, USA: McGraw-Hill, Inc.

Wilms, P., Wieringa, J., Blijdenstein, T. et al. 2022. On the Difficulty of Determining the Apparent Wall Slip of Highly Concentrated Suspensions in Pressure Driven Flows: The Accuracy of Indirect Methods and Best Practice. *J Non-newton Fluid Mech* **299**. https://doi.org/10.1016/j.jnnfm.2021.104694.